

Influence of Dielectric Overlay Permittivity on Size and Performance of Miniaturized ESPAR Antenna

M. Czelen¹, M. Rzymowski², *Member, IEEE*, K. Nyka³, *Senior Member, IEEE*, and L. Kulas⁴, *Senior Member, IEEE*
Department of Microwave and Antenna Engineering
Faculty of Electronics, Telecommunications and Informatics, Gdansk University of Technology
 Gdansk, Poland

¹ mateusz.czelen@pg.edu.pl, ² mateusz.rzymowski@pg.edu.pl, ³ krzysztof.nyka@pg.edu.pl, ⁴ lukasz.kulas@pg.edu.pl

Abstract—In this paper, influence of dielectric overlay permittivity on miniaturized ESPAR antenna parameters is presented. ESPAR antenna is a low-cost and energy-efficient way to implement beam steering capability to a node and improve network performance. The antenna size reduction is obtained by embedding its active and passive elements in ABS based materials of relative permittivity equal to 4, 5.5 and 7.5 in order to achieve network node compact size. Simulation results of three optimized for particular dielectric constant designs are presented and tradeoff between dimensions reduction and performance is discussed. Selected materials and antenna design are dedicated to be fabricated in 3D print technology, so can be easily prototyped.

Keywords—reconfigurable antenna, antenna miniaturization, 3D printing, switched-beam antenna, steerable antenna, electronically steerable parasitic array radiator (ESPAR) antenna

I. INTRODUCTION

The principle of electronically steerable parasitic array radiator (ESPAR) antenna operation relies on controlling its radiation pattern by changing load impedances in passive elements' ports while a single active element acts as an active radiator [1]. The active element is surrounded by number of passive ones which are terminated with electronically steerable reactances. ESPAR antennas are characterized by lower complexity, cost and power consumption than conventional phased array [2]. One of the most popular types of ESPAR antennas consists of monopoles mounted on a circular ground plane, since it simplifies antenna's construction and the design of loading impedance steering circuits [3].

Usually in such antenna analog voltage control pin diodes or varactors are used to realize variable loads. A different approach is presented in [4], [5] where passive monopoles' ends are connected to single-pole double-throw (SPDT) switches, which provide dual-state control by shorting selected elements to the ground and leaving the rest of them open. This results in a directional radiation pattern and allows for steering its horizontal direction using only digital input-output (DIO) ports. Such simplification allows the antenna to be integrated with simple microcontroller being part of a wireless sensor network (WSN) node. In consequence, such nodes obtain new useful features like a beam steering, direction of arrival (DoA) estimation and localization functionalities which results in improving energy

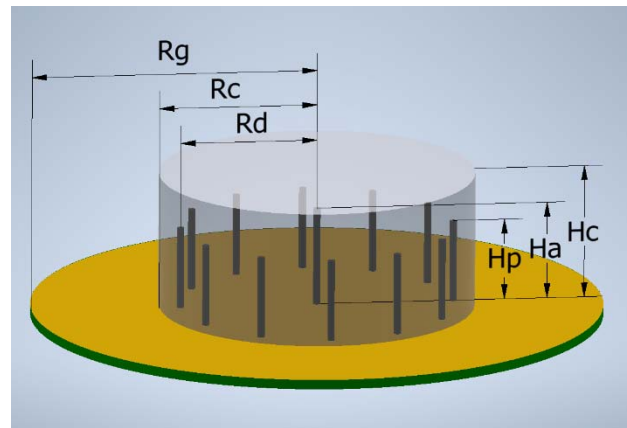


Fig. 1. Miniaturized ESPAR antenna structure

efficiency, coverage and connectivity of the network [5-7]. It can be beneficial for number types of networks, particularly in precision farming applications where energy efficiency, big network coverage and compact size is required [8], [9].

Size of the ESPAR antenna is an important issue when integrating with WSN nodes and especially when it is dedicated for a drone of limited payload space. There is a number of papers concerning ESPAR antenna miniaturization [11], [12]. In [11] the authors achieved miniaturization by embedding antenna in a homogenous dielectric material. The similar concept was employed in [12] to fabricate antenna at lower cost using 3D print technology. In order to manufacture dielectric overlay, cheap and common polylactic acid (PLA) filament of $\epsilon_r = 2.74$ has been used resulting in 23% radius reduction. This corresponds to the antenna base radius of 59 mm for 2.4 GHz band, which in some applications may still be too large.

In this paper we investigate the effects of further size reduction by using 3D print materials of higher permittivity and present their influence on antenna performance. In particular, we consider tradeoffs between size and antenna parameters like gain or bandwidth. To this end, three miniaturized ESPAR antennas with different permittivity overlay material have been designed and compared. The paper also presents a novel way of impedance matching in such type of antennas.

II. ANTENNA CONCEPT AND DESIGN

Antenna design is based on the one presented in [5]. The basis of the antenna is a circular ground plane realized as a top layer of the FR4 substrate, on which a single, active monopole and 12 parasitic elements are mounted. Connecting each parasitic element to the SPDT switch allows one to change its

This work was supported in part by the AFARCLOUD Project through the ECSEL Joint Undertaking (JU) under grant agreement No 783221 and in part by the European Union's Horizon 2020 research and innovation programme and Austria, Belgium, Czech Republic, Finland, Germany, Greece, Italy, Latvia, Norway, Poland, Portugal, Spain, Sweden.

function from director to reflector and vice versa by loading it with open or short circuit. In the proposed antenna design, opening five consecutive and shorting remaining seven passive monopoles allows to obtain a directional radiation pattern with maximum gain aligned with the third open element position. In consequence, flexible beam steering capability is achieved and utilization of SPDT switches simplifies the steering circuit.

Antenna size reduction is achieved by embedding all radiators in a cylindrical shaped dielectric overlay. This technique was proposed in [11] and adopted to the 3D print technology in [12]. In both cases, it provided satisfactory results, confirmed by realization and measurements. This article explores the possibility of further size reduction achieved by higher permittivity filaments than PLA and examines their influence on the antenna performance. The antennas have been designed to have their overlays fabricated in 3D print technology and air gaps between antenna elements and dielectric structure investigated in [12] were included. This feature allows for more realistic designs and improved agreement between simulation and measurement results. The proposed antenna structure is shown in Fig. 1.

When modeling load impedances of passive elements one should note that the realistic values are far from the ideal short and open circuit. For that reason, in order to get accurate results, the impedances in both switch states have been determined by simulation of realistic switching circuit layout using Advanced Design System (ADS) software. The obtained impedance values, $(26.8 - j208.5) \Omega$ for open and $(2 - j29.3) \Omega$ for short state, were included in the antenna simulation model.

Introducing higher permittivity materials for fabrication of dielectric cylinder revealed a new design problem, which is providing a satisfactory shape of radiation pattern along with good impedance matching. Reflection coefficient decrease to an acceptable level is achieved at a cost of degradation of far-field characteristics. Hence, to mitigate this trade-off, additional matching by means of a slot between active element and ground plane has been proposed (Fig. 2). Its meander layout was determined by the SMA connector PCB footprint. Impedance matching can be achieved by modification of the total slot length L_s . The effect of including variable length matching slot in antenna model by means of input impedance are depicted in Fig. 3.

The matching slot changes the input impedance in a way unachievable by simple modification of the active element's height H_a , which thus in some cases can help to match the antenna. In this design, proper selection of slot dimensions and active element height resulted in minimization of reflection coefficient, while maintaining radiation pattern nearly unchanged. However, since the input impedance depends not only on H_a but also on other antenna dimensions, the design of the matching slot size has to be included in the optimization process. Similar, yet different, ways of input impedance modifications were introduced in the literature, e.g. in [13] where dual bandwidth operation of ESPAR antenna was needed authors used additional matching posts near active element. The advantage of the solution presented in this paper is that there is no need to manufacture and mount additional elements and only a simple modification of PCB layout is required.

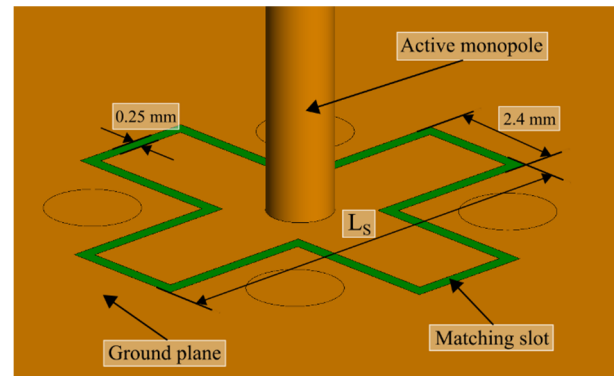


Fig. 2. Impedance matching slot structure.

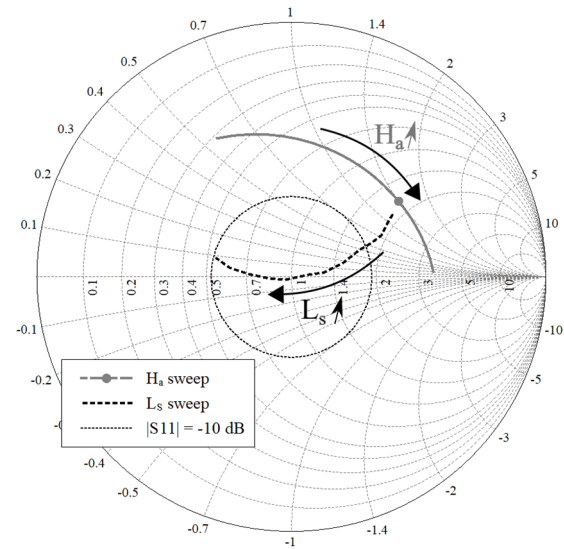


Fig. 3. Normalized input impedance at 2.45 GHz as a function of impedance matching slot size and active element length.

III. SIMULATION RESULTS

Three versions of antenna with different permittivity of overlay material have been designed in order to get more complete evaluation of its influence on antenna parameters. The choice of dielectric constant values was determined by the availability of corresponding filaments on the market. The ABS based PREPERM materials of dissipation factor equal to 0.004 and relative permittivity ϵ_r of 4.0, 5.5 and 7.5 have been chosen.

All three antenna versions were designed using FEKO software where the global response surface method (GRSM) was used for optimization in which the goals were set to minimize the side lobe level (SLL) and maximize antenna gain while providing a satisfactory level of the reflection coefficient. The simulation results are presented in Fig. 4 for radiation pattern in the elevation plane and in Fig. 5 for the reflection coefficient. Table I compares dimensions (in millimeters and free space wavelengths λ_0) of three designed antennas with the standard-size [5] and PLA based [12] versions.

In all three cases, a directive radiation pattern with relatively low back radiation and impedance matching have been obtained. Antenna dimensions are decreasing with increase of permittivity. The smallest reduction ratio is observed in case of H_a and H_p . It is a consequence of the air gaps around monopoles, but their presence has minor impact on the biggest antenna dimension R_g .

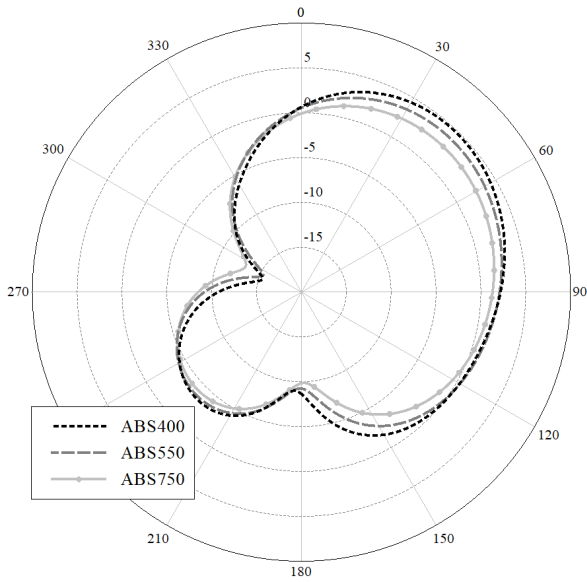


Fig. 4. Antenna radiation pattern in elevation plane at 2.45 GHz for different overlay permittivities [dBi]

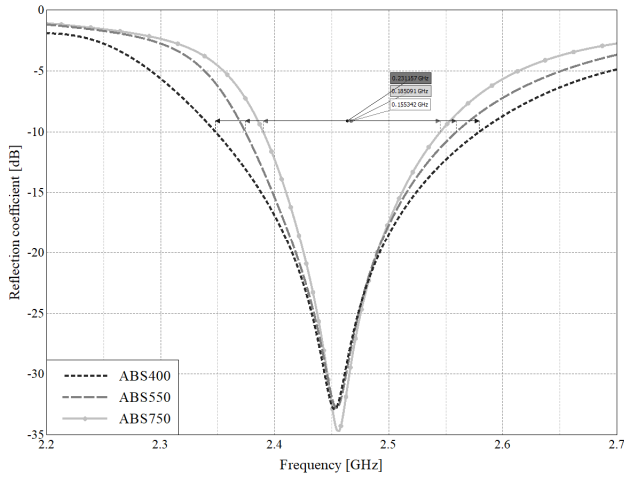


Fig. 5. Antenna reflection coefficient as a function of frequency for different overlay permittivities [dB]

TABLE I. DIMENSIONS COMPARISON OF DIFFERENT PERMITTIVITY ESPAR ANTENNA VERSIONS

	STD[5]		PLA[12]		ABS400		ABS550		ABS750	
	[mm]	$[\lambda_0]$	[mm]	$[\lambda_0]$	[mm]	$[\lambda_0]$	[mm]	$[\lambda_0]$	[mm]	$[\lambda_0]$
ϵ_r	1		2.74		4		5.5		7.5	
R_g	76.2	0.62	59	0.48	49	0.4	41.7	0.34	35.9	0.29
R_d	45	0.37	28.2	0.23	20.2	0.17	15.9	0.13	15.1	0.12
H_a	24.1	0.2	20.4	0.17	19.4	0.16	18.9	0.15	19.4	0.16
H_p	28.5	0.23	16.8	0.14	14.4	0.12	12.6	0.1	11.3	0.09
R_c	-	-	32.6	0.27	23.4	0.19	19.4	0.16	18.6	0.15
H_c	-	-	24.4	0.2	20.6	0.17	18.6	0.15	16.8	0.14

IV. PARAMETERS COMPARISON

The main comparison criteria are antenna peak gain, impedance bandwidth and size reduction factor which is calculated as antenna base radius reduction relative to the standard-size antenna. These and some other parameters are presented in Table II.

TABLE II. PARAMETERS COMPARISON OF DIFFERENT PERMITTIVITY ESPAR ANTENNA VERSIONS

	STD[5]	PLA[12]	ABS400	ABS550	ABS750
Dielectric constant	1	2.74	4	5.5	7.5
Size reduction ratio	-	0.23	0.36	0.45	0.53
Peak gain [dBi]	8.2	5.7	4.8	3.9	2.7
Bandwidth [MHz]	284	276	231	185	155
Reflection coefficient @ 2.45 GHz [dB]	-16	-31	-33	-32	-32
Efficiency [%]	91.5	81.5	85.4	83.9	72
HPBW @ $\varphi = 0^\circ$ [°]	65.1	82.2	89.2	110.7	120.2
HPBW @ $\theta = 90^\circ$ [°]	76.2	108.3	143.7	168.3	192.6

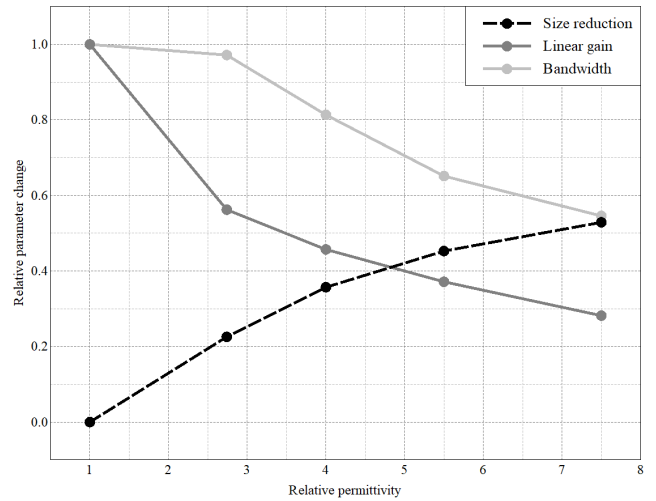


Fig. 6. Size reduction, linear gain and bandwidth relative to standard-size antenna parameters as a function of overlay relative permittivity

Introducing higher permittivity materials allows for successful size reduction which is larger than in the PLA version. As it was expected, the main costs of increasing overlay permittivity are gain and bandwidth decrease. The latter is also affected by the matching slot. Approximate gain decrease is equal to 1.2 dBi per centimeter of radius reduction. A decision about gain and size trade-off has to be made depending on the particular application. The above presented comparison of expected performance for specific size reduction can help to make this decision. Additionally, Fig. 6 presents relative to standard-size antenna parameters change in function of relative permittivity.

V. CONCLUSIONS

In this paper, the influence of dielectric overlay permittivity on miniaturized ESPAR antenna parameters has been presented. Three versions of the antenna based on available 3D print filaments with overlay dielectric constant of 4.0, 5.5 and 7.7 have been designed achieving base radius reduction factor equal to 0.36, 0.45 and 0.53, respectively. The difficulty of providing simultaneously desired radiation pattern and impedance matching has been overcome by introducing the matching slot around the feed of the active element. The proper selection of its dimensions allows one to minimize reflection coefficient with no impact on radiation pattern. Increasing overlay permittivity, besides size reduction, also affects antenna performance, mainly in terms of peak gain and bandwidth. Compromising these two effects

should depend on particular antenna application. Some energy-efficient systems may require certain communication range, which implicates minimum antenna gain requirement and in the others priority will be possibly small size of WSN node. This article, by presenting trade-offs for different configuration, can help to make an optimal decision as to the design assumptions.

ACKNOWLEDGMENT

The authors would like to thank the Academic Computer Centre in Gdansk, Poland (TASK) where all the calculations were carried out.

REFERENCES

- [1] R. Harrington, "Reactively controlled directive arrays," *IEEE Trans. Antennas Propag.*, vol. AP-26, no. 3, pp. 390-395, May 1978.
- [2] H. Kawakami and T. Ohira, "Electrically steerable passive array radiator (ESPAR) antennas," *IEEE Antennas Propag. Mag.*, vol. 47, no. 2, pp. 43-50, April 2005.
- [3] R. Schlub and D. V. Thiel, "Switched parasitic antenna on a finite ground plane with conductive sleeve," *IEEE Trans. Antennas Propag.*, vol. 52, no. 5, pp. 1343-1347, May 2004.
- [4] M. Rzymowski, P. Woznica and L. Kulas, "Single-anchor indoor localization using ESPAR antenna," *IEEE Antennas Wireless Propag. Lett.*, vol. 15, pp. 1183-1186, 2016.
- [5] L. Kulas, "RSS-based DoA estimation using ESPAR antennas and interpolated radiation patterns," *IEEE Antennas Wireless Propag. Lett.*, vol. 17, pp.25-28, 2018.
- [6] F. Viani, L. Lizzi, M. Donelli, D. Pregolato, G. Oliveri, and A. Massa, "Exploitation of parasitic smart antennas in wireless sensor networks," *J. Electromagn. Waves Appl.*, vol. 24, no. 7, pp. 993-1003, Jan. 2010.
- [7] T. N. Le, A. Pegatoquet, T. Le Huy, L. Lizzi and F. Ferrero, "Improving energy efficiency of mobile WSN using reconfigurable directional antennas," *IEEE Commun. Lett.*, vol. 20, no. 6, pp. 1243-1246, June 2016.
- [8] H. Jawad, R. Nordin, S. Jawad, and M. Ismail, "Energy-efficient wireless sensor networks for precision agriculture: A review," *Sensors*, vol. 17, no. 8, 2017, Art. no. E1781.
- [9] R. MacRuairi, M. T. Keane and G. Coleman, "A wireless sensor network application requirements taxonomy," *Proc. 2nd Int. Conf. Sens. Technol. Appl.*, Cap Esterel, 2008, pp. 209-216
- [10] H. Liu, S. Gao and T. H. Loh, "Compact-size electronically steerable parasitic array radiator antenna," *Proc. Loughborough Antennas Propag. Conf. (LAPC)*, Loughborough, 2009, pp. 265-268.
- [11] Junwei Lu, D. Ireland and R. Schlub, "Dielectric embedded ESPAR (DE-ESPAR) antenna array for wireless communications," *IEEE Trans. Antennas Propag.*, vol. 53, no. 8, pp. 2437-2443, Aug. 2005.
- [12] M. Czelen, M. Rzymowski, K. Nyka and L. Kulas, "Miniaturization of ESPAR antenna using low-cost 3D printing process," in press
- [13] O. Shibata and T. Furuhi, "Dual-band ESPAR antenna for wireless LAN applications," *Proc. IEEE Antennas Propag. Soc. Int. Symp.*, Washington, DC, 2005, pp. 605-608 vol. 2B.

